Structural Engineering and Mechanics, *Vol. 61, No. 6 (2017) 765-773*
DOI: https://doi.org/10.12989/sem.2017.61.6.765

Quadratic B-spline finite element method for a rotating non-uniform Rayleigh beam

Vijay Panchore and Ranjan Ganguli*

Aerospace Engineering, Indian Institute of Science, Bangalore, India

(Received June 16, 2016, Revised November 22, 2016, Accepted November 23, 2016)

Abstract. The quadratic B-spline finite element method yields mass and stiffness matrices which are half the size of matrices obtained by the conventional finite element method. We solve the free vibration problem of a rotating Rayleigh beam using the quadratic B-spline finite element method. Rayleigh beam theory includes the rotary inertia effects in addition to the Euler-Bernoulli theory assumptions and presents a good mathematical model for rotating beams. Galerkin's approach is used to obtain the weak form which yields a system of symmetric matrices. Results obtained for the natural frequencies at different rotating speeds show an accurate match with the published results. A comparison with Euler-Bernoulli beam is done to decipher the variations in higher modes of the Rayleigh beam due to the slenderness ratio. The results are obtained for different values of non-uniform parameter ($\bar{n}$).

Keywords: Galerkin method; quadratic B-spline basis function; rotating beam; free vibration; conventional finite element method

1. Introduction

B-spline curves and surfaces are widely used for computer aided design purposes (Zeid 2007). The local control is an achievable task with these curves. This characteristic is compatible with the finite element method where lower order polynomials are used for the trial and test function approximation. B-spline basis functions are constructed from lower order polynomials and applied with the finite element approach based on the continuity requirement of the problem: the linear B-spline basis function are used for the C^0 continuity requirement, the quadratic B-spline basis function for the C^1 continuity requirement, etc. In this work, we focus on a Rayleigh beam problem and the combination of the quadratic B-spline basis function with the finite element approach is selected to showcase its advantage over the conventional finite element method.

The quadratic B-spline finite element formulation is advantageous over the conventional finite element method: the size of mass and stiffness matrix is reduced to half when compared to conventional approach, it does not require a mesh, and a lower polynomial order is required for approximation when compared to conventional approximation. These characteristics can be useful for many applications; problems involving large systems and cracks within the continuum. A combined approach for computer aided design and analysis can also be performed with B-spline curves.

In the finite element method, Galerkin's approach is often used to obtain the weak form where trial and test function are formulated from the same basis function and this approach yields a system of symmetric matrices (Reddy 2005); the natural boundary conditions are satisfied while formulating the weak form and the essential boundary conditions are satisfied while solving the algebraic equations using a transformation matrix (Shen *et al.* 2014). Since the quadratic B-spline basis function is a lower order polynomial, the numerical solutions of a rotating Rayleigh beam problem with the Galerkin quadratic B-spline finite element method are most likely to converge.

Mostly, Euler-Bernoulli beam theory is used for structures such as the rotating blade. The advantages of this approach include: formulation of a single uncoupled differential equation, straight forward approach in numerical solutions, and reasonable accuracy with less computational effort. Timoshenko beam theory, however, includes shear deformation and rotary inertia. This yields a coupled differential equation. However, it includes additional complexity; shear locking in numerical solutions. Instead, Rayleigh beam theory includes only rotary inertia term in addition to Euler-Bernoulli assumptions. In Rayleigh theory, only a single differential equation is formulated. This incorporates additional accuracy with a straight forward approach in numerical solutions. The slenderness ratio $\left(r = \sqrt{A_0 R^2 / I_0}\right)$, which is explained in the later part of this paper, is a differentiating factor between Euler-Bernoulli beam and Rayleigh beam results. At low slenderness ratio, higher natural frequencies of Rayleigh beam and Euler-Bernoulli beam tend to differ; rotary inertia plays a prominent role in higher modes as the curvature of bending will be higher (Avcar 2015, Tang *et al.* 2015). Rayleigh beam theory is the missing link between Euler-Bernoulli and Timoshenko beam theory and has

*Corresponding author, Professor
E-mail: drganguli@gmail.com

ISSN: 1225-4568 (Print), 1598-6217 (Online)

considerable practical and pedagogical value. Recently, closed form solutions for axially loaded Rayleigh beams have been obtained (Sarkar *et al.* 2016).

Generally, the free vibration problem of a rotating beam is solved using the finite element method (Hodges and Rutkowski 1981, Nagaraj and Shanthakumar 1975, Bauchau and Hong 1987, Hoa 1979). Various attempts have been made to get the analytical solutions assuming simplifications to the equation (Bokaian 1990). The power series solution of the differential equation was obtained using the Frobenius method (Giurgiutiu and Stafford 1977). Mao (2015) used the Adomain modified decomposition method to convert the governing differential equation of a rotating tapered beam into a recursive algebraic equation. Mohammadnejad (2015) addressed vibration problems including a Rayleigh beam with variable axial force. He performed repeated integrations to convert the governing ordinary differential equation into weak form integral equations and compared the numerical results with published literature and finite element method results. The free vibration problem of a rotating Rayleigh beam can be solved with the finite element formulation. In literature, this problem has been addressed with semi-analytical and numerical solutions. A series solution was obtained using the Frobenius method, the dynamic stiffness matrix is derived in the process before applying the Wittrick-Williams algorithm to calculate natural frequencies, and the results were obtained for the various slenderness ratios to capture the change in higher modes (Banerjee and Jackson 2013). The Rayleigh-Ritz method along with the cell discretization method has also been used to solve the rotating Rayleigh beam problem (Auciello 2013). However, B-spline finite element solutions remain to be explored for this problem.

The B-spline basis functions have been used with different methods of weighted residuals. The regularized long wave equation was solved with the combination of least square method and cubic B-spline basis function (Dag and Ozer 2001). The same equation has also been solved with the combination of Galerkin method and quadratic B-spline basis function (Gardner *et al.* 2013). A different approach, a method of subdivision-based spline curves, shows better convergence than the uniform refinement with lesser number of elements for geometrically non-linear problems (Bornemann and Cirak). A time integration scheme has also been introduced with B-spline curves where the method was found to be conditionally stable (Rostami *et al.* 2013). A combined approach was used for the design and analysis with B-spline approximation, where the spectral element method and the B-spline finite element method were used for the rod and plate model, and no major difference was observed between these two methods. For better convergence, three refinements were discussed as well: *n*-refinement, increased number of B-spline curves; *p*-refinement, variation in the degree of curves; *k*-refinement, knot alteration (Kagan *et al.* 1998).

The cubic B-spline finite element method was applied to the analysis of thin symmetric shells, where the cubic B-spline was used for the first time to interpolate both the displacement and geometry. The advantages over the conventional finite elements were shown as well; stresses are continuous at nodes and the cubic B-spline interpolation are superior to the Hermite interpolation where the second derivative of the field variable is not continuous (Gupta *et al.* 1991). Isogeometric analysis uses non-uniform rational B-spline basis functions and the idea is to have a combined approach in analysis and design, which leads to convenience from the industrial perspective. It is a potential alternative to the conventional finite element method (Hughes *et al.* 2005). Higher order B-splines curves are also used frequently in research. Higher accuracy was achieved with the cubic and quintic B-spline functions for the static analysis of flat cylindrical shell (Shen and Wang 1987). A sextic B-spline collocation method was recently used for a non-rotating Euler-Bernoulli beam (Mohammadi 2014).

In this paper, the quadratic B-spline finite element method is used to solve the rotating Rayleigh beam free vibration problem. Equations are also represented in non-dimensional form for the purpose of convenience. The mass and stiffness matrix are derived for both the approaches; B-spline finite element method and finite element method, results are obtained with these methods as well. A subinterval in B-spline approximation equals an element in finite element approximation. Results are obtained for the cantilever boundary condition with an equivalent approximation for both the methods; total 40 subintervals in B-spline method and 40 elements in finite element method. Results are obtained at different slenderness ratio for Rayleigh beam. Results are also obtained with Euler-Bernoulli beam theory, where the slenderness ratio plays no role in the formulation. The results show that the quadratic B-spline finite element method presents a computationally efficient alternative to the conventional finite element method. Lower order models can be created using the B-spline finite element which can be useful for control applications involving rotating beams (Wang and Wereley 2004). To the best of our knowledge, this is the first paper which illustrates the B-spline finite element method for rotating beams.

2. Weak formulation of the governing differential equation

The Rayleigh beam theory includes an additional rotary inertia term when compared to Euler-Bernoulli beam theory. This results in a single differential equation. A rotating beam differential equation includes a centrifugal force term in addition to a non-rotating beam differential equation which varies along the length of the beam; analytical solutions are difficult to obtain for the rotating Rayleigh beam differential equation. In this section, we derive the mass and stiffness matrix of a beam with varying cross section and varying stiffness.

The governing differential equation of a rotating Rayleigh beam is given by (Banerjee and Jackson 2013)

$$\frac{\partial^2}{\partial x^2}\left[EI(x)\frac{\partial^2 w(x,t)}{\partial x^2}\right] + \rho A(x)\frac{\partial^2 w(x,t)}{\partial t^2} - \frac{\partial}{\partial x}\left[G(x)\frac{\partial w(x,t)}{\partial x}\right]$$

$$+\frac{\partial}{\partial x}\left\{\rho I(x)\frac{\partial}{\partial x}\left[\Omega^2 w(x,t)-\frac{\partial^2 w(x,t)}{\partial t^2}\right]\right\} \quad (1)$$
$$=0$$

Here, $EI(x)$ is the flexural stiffness, ρ is the density, $A(x)$ is the area of cross section, $w(x)$ is the transverse displacement and $G(x)$ is the centrifugal force which is given by

$$G(x)=\int_x^R \rho A(x)\Omega^2 x\,dx \quad (2)$$

where, Ω is the angular velocity and R is the radius of the rotating beam. The term involving $\rho I(x)$ in Eq. (1) is the additional term which occurs in Rayleigh beam theory, when compared to Euler-Bernoulli beam theory.

For the free vibration problem, we assume $w(x,t)=e^{i\omega t}\overline{w}(x)$ to get

$$\frac{d^2}{dx^2}\left[EI(x)\frac{d^2\overline{w}(x)}{dx^2}\right]-\omega^2\rho A(x)\overline{w}(x)$$
$$-\frac{d}{dx}\left[G(x)\frac{d\overline{w}(x)}{dx}\right]+\frac{d}{dx}\left\{\rho I(x)\frac{d}{dx}\left[(\Omega^2+\omega^2)\overline{w}(x)\right]\right\}=0 \quad (3)$$

The weak formulation of Eq. (3) is given by

$$\int_0^R v(x)\left\{\begin{array}{l}\dfrac{d^2}{dx^2}\left[EI(x)\dfrac{d^2\overline{w}(x)}{dx^2}\right]\\ -\rho A(x)\omega^2\overline{w}(x)\\ -\dfrac{d}{dx}\left[G(x)\dfrac{d\overline{w}(x)}{dx}\right]\end{array}\right\}dx \quad (4)$$
$$+\int_0^R v(x)\frac{d}{dx}\left\{\rho I(x)\frac{d}{dx}\left[(\Omega^2+\omega^2)\overline{w}(x)\right]\right\}=0$$

Integrating Eq. (4) by parts, we get

$$\left|v(x)\left\{\begin{array}{l}\dfrac{d}{dx}\left[EI(x)\dfrac{d^2\overline{w}(x)}{dx^2}\right]\\ -G(x)\dfrac{d\overline{w}(x)}{dx}\\ +\rho I(x)\dfrac{d}{dx}\left[(\Omega^2+\omega^2)\overline{w}(x)\right]\end{array}\right\}\right|_0^R$$
$$-\left|\frac{dv(x)}{dx}EI(x)\frac{d^2\overline{w}(x)}{dx^2}\right|_0^R$$
$$+\int_0^R EI(x)\frac{d^2v(x)}{dx^2}\frac{d^2\overline{w}(x)}{dx^2}dx+\int_0^R G(x)\frac{dv(x)}{dx}\frac{d\overline{w}(x)}{dx}dx$$
$$-\Omega^2\int_0^R \rho I(x)\frac{dv(x)}{dx}\frac{d\overline{w}(x)}{dx}dx$$
$$-\omega^2\int_0^R \rho A(x)v(x)\overline{w}(x)dx-\omega^2\int_0^R \rho I(x)\frac{dv(x)}{dx}\frac{d\overline{w}(x)}{dx}dx=0 \quad (5)$$

The first two terms of Eq. (5), which are outside the integrals, will reduce to zero; the test function satisfies the essential boundary conditions. The natural boundary conditions will be satisfied in the first two terms as well, and are given by

$$\left\{\begin{array}{l}\dfrac{d}{dx}\left[EI(x)\dfrac{d^2\overline{w}(x)}{dx^2}\right]-G(x)\dfrac{d\overline{w}(x)}{dx}\\ +\rho I(x)\dfrac{d}{dx}\left[(\Omega^2+\omega^2)\overline{w}(x)\right]\end{array}\right\}\Bigg|_{(x=R)}=0 \quad (6)$$

$$EI(x)\frac{d^2\overline{w}(x)}{dx^2}\Bigg|_{(x=R)}=0 \quad (7)$$

The left hand side of Eqs. (6) and (7) represent the shear force and bending moment at the tip of a rotating Rayleigh beam, respectively.

Eq. (5) can be rewritten as

$$\int_0^R EI(x)\frac{d^2v(x)}{dx^2}\frac{d^2\overline{w}(x)}{dx^2}dx+\int_0^R G(x)\frac{dv(x)}{dx}\frac{d\overline{w}(x)}{dx}dx$$
$$-\Omega^2\int_0^R \rho I(x)\frac{dv(x)}{dx}\frac{d\overline{w}(x)}{dx}dx-\omega^2\int_0^R \rho A(x)v(x)\overline{w}(x)dx- \quad (8)$$
$$\omega^2\int_0^R \rho I(x)\frac{dv(x)}{dx}\frac{d\overline{w}(x)}{dx}dx-0$$

The conventional finite element formulation involves Hermite interpolation of trial and test function and it is given by

$$\overline{w}(x)=[N(x)][q] \quad (9)$$

$$v(x)=[\delta q]^T[N(x)]^T \quad (10)$$

Substituting Eqs. (9) and (10) in equation (8), we get

$$\left[\int_0^R EI(x)\frac{d^2[N]^T}{dx^2}\frac{d^2[N]}{dx^2}dx\right][q]+$$
$$\left[\int_0^R G(x)\frac{d[N]^T}{dx}\frac{d[N]}{dx}dx-\Omega^2\int_0^R \rho I(x)\frac{d[N]^T}{dx}\frac{d[N]}{dx}dx\right][q]$$
$$-\left[\omega^2\int_0^R \rho A(x)[N]^T[N]dx+\omega^2\int_0^R \rho I(x)\frac{d[N]^T}{dx}\frac{d[N]}{dx}dx\right][q]=0 \quad (11)$$

where, $[N(x)]$ represents the shape function vector and $[q]$ represents a vector containing nodal degrees of freedom.

From Eq. (11), the stiffness matrix can be written as

$$[K]=\int_0^R EI(x)\frac{d^2[N]^T}{dx^2}\frac{d^2[N]}{dx^2}dx$$
$$+\int_0^R G(x)\frac{d[N]^T}{dx}\frac{d[N]}{dx}dx-\Omega^2\int_0^R \rho I(x)\frac{d[N]^T}{dx}\frac{d[N]}{dx}dx \quad (12)$$

and the mass matrix can be written as

$$[M]=\int_0^R \rho A(x)[N]^T[N]dx+\int_0^R \rho I(x)\frac{d[N]^T}{dx}\frac{d[N]}{dx}dx \quad (13)$$

To get the stiffness and mass matrix of a rotating Euler-Bernoulli beam, the terms involving $\rho I(x)$ have to be omitted; the third term in Eq. (12) and the second term in Eq. (13) will not contribute to a rotating Euler-Bernoulli stiffness and mass matrix, which are given by

$$[K]_{E-B}=\int_0^R EI(x)\frac{d^2[N]^T}{dx^2}\frac{d^2[N]}{dx^2}dx+\int_0^R G(x)\frac{d[N]^T}{dx}\frac{d[N]}{dx}dx \quad (14)$$

$$[M]_{E-B}=\int_0^R \rho A(x)[N]^T[N]dx \quad (15)$$

The stiffness and mass matrix terms are straightforward in Rayleigh beam theory and Euler-Bernoulli beam theory, where matrices are easy to invert and are of lower size. However, in Timoshenko beam theory, the size of matrices will be even higher (based on the interpolation) and matrices will be difficult to invert; the enhanced accuracy is achieved at higher computational cost and with an additional problem of shear locking.

Natural frequencies of a rotating Rayleigh beam are given by

$$\omega^2[M][\phi]=[K][\phi] \quad (16)$$

where, i=1,2,3…N, where, ω_1 is the first natural frequency and $[\phi]$ is an eigenvector.

3. Non-dimensional form of the equation

Non-dimensional form of equation simplifies the formulation as various parameters can be clubbed together into a few key parameters. A non-uniform beam has the varying cross-section and stiffness across its length. To obtain the non-dimensional form of a non-uniform beam, we consider variations in cross sectional area and second moment of area, given by (Banerjee and Jackson 2013)

$$I(x)=I_0 g(x),\ A(x)=A_0 f(x) \quad (17, 18)$$

where,

$$g(x)=\left(1-c\frac{x}{R}\right)^{\bar{n}+2},\ f(x)=\left(1-c\frac{x}{R}\right)^{\bar{n}} \quad (19, 20)$$

and c is a constant which can be considered as the taper ratio. Here, A_0 and I_0 are the cross sectional area and second moment of area terms, respectively, at the left end (thick end) of the beam. By considering different values of the non-uniform parameter $\bar{n}$, various practical cases of tapered beams can be created.

The non-dimensional form of the Eq. (3) is given by

$$\frac{d^2}{d\zeta^2}\left[g(\zeta)\frac{d^2\bar{w}(\zeta)}{d\zeta^2}\right]-\lambda^2 f(\zeta)\bar{w}(\zeta)$$
$$-s^2\frac{d}{d\zeta}\left[h(\zeta)\frac{d\bar{w}(\zeta)}{d\zeta}\right]+\frac{s^2}{r^2}\frac{d}{d\zeta}\left[g(\zeta)\frac{d\bar{w}(\zeta)}{d\zeta}\right]$$
$$+\frac{\lambda^2}{r^2}\frac{d}{d\zeta}\left[g(\zeta)\frac{d\bar{w}(\zeta)}{d\zeta}\right]=0 \quad (21)$$

where, $\zeta=\frac{x}{R}$, $r^2=\frac{A_0R^2}{I_0}$, $s^2=\Omega^2\frac{\rho A_0R^4}{EI_0}$, $\lambda^2=\omega^2\frac{\rho A_0R^4}{EI_0}$,

and $h(\zeta)=\int_\zeta^1 \zeta f(\zeta)d\zeta$.

Here, s is the non-dimensional rotating speed, λ is the non-dimensional natural frequency, and r is the slenderness ratio which differentiates results of the Rayleigh beam and the Euler-Bernoulli beam. For a thick beam, the results of both the theories tend to differ, but as the beam gets slender the difference is insignificant. For a thick beam, Timoshenko beam theory enhances the results further by adding the shear deformation term into the formulation.

In non-dimensional form, the boundary conditions are given by

$$\bar{w}(\zeta)\big|_{(\zeta=0)}=0,\left.\frac{d\bar{w}(\zeta)}{d\zeta}\right|_{(\zeta=0)}=0, \quad (22, 23)$$

$$\left\{\frac{d}{d\zeta}\left[g(\zeta)\frac{d^2\bar{w}(\zeta)}{d\zeta^2}\right]-s^2h(\zeta)\frac{d\bar{w}(\zeta)}{d\zeta}+\frac{\left(s^2+\lambda^2\right)}{r^2}g(\zeta)\frac{d\bar{w}(\zeta)}{d\zeta}\right\}\Bigg|_{(x=R)}=0 \quad (24)$$

$$g(\zeta)\left.\frac{d^2\bar{w}(\zeta)}{d\zeta^2}\right|_{(x=R)}=0 \quad (25)$$

From the weak formulation of Eq. (21), we can obtain the stiffness matrix as

$$[K]=\int_0^1 g(\zeta)\frac{d^2[N]^T}{d\zeta^2}\frac{d^2[N]}{d\zeta^2}d\zeta$$
$$+\int_0^1 s^2h(\zeta)\frac{d[N]^T}{d\zeta}\frac{d[N]}{d\zeta}d\zeta-\int_0^1\frac{s^2}{r^2}g(\zeta)\frac{d[N]^T}{d\zeta}\frac{d[N]}{d\zeta}d\zeta \quad (26)$$

and the mass matrix as

$$[M]=\int_0^1 f(\zeta)[N]^T[N]d\zeta+\int_0^1\frac{1}{r^2}g(\zeta)\frac{d[N]^T}{d\zeta}\frac{d[N]}{d\zeta}d\zeta \quad (27)$$

From Eqs. (26) and (27), we notice that as the value of the slenderness ratio $\left(\sqrt{A_0R^2/I_0}\right)$ increases, the results of the Rayleigh beam will approach to the results of the Euler-Bernoulli beam; the third term in Eq. (26) and second term in Eq. (27) will be omitted in Euler-Bernoulli beam theory. For a non-rotating beam formulation, one has to substitute the value of non-dimensional rotating speed (s) equal to zero; the second and third terms of the stiffness matrix will be omitted.

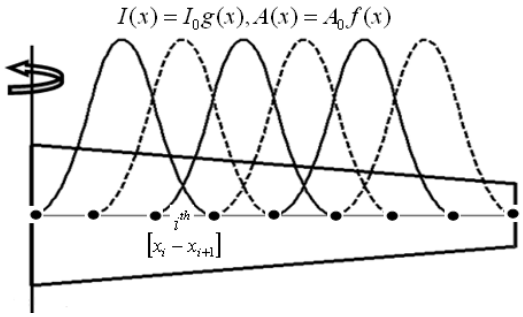

Fig. 1 Quadratic B-spline curves

4. Quadratic B-spline finite element formulation

The B-spline curves are chosen with the finite element approach based on the continuity requirement of the problem. In conventional finite element method, the Hermite interpolation is an appropriate selection for the Rayleigh beam problem, where displacement and slope are continuous at the nodal boundaries. Similarly, in B-spline finite element method, the quadratic B-spline curves satisfy the required C^1 continuity.

The Hermite interpolation requires two points while the quadratic B-spline curve requires four points for interpolation; three B-spline curves contribute to one subinterval and vice-versa. A combined approach of design and analysis can be performed with these curves. Fig. 1 shows a non-uniform rotating Rayleigh beam with the quadratic B-spline curve distribution.

The B-spline basis function for the zeroth order polynomial (p=0) is given by

$$\phi_{i,0}(x) = \begin{cases} 1 & if \quad x_i \le x \le x_{i+1} \\ 0 & otherwise \end{cases} \tag{28}$$

To calculate higher order B-spline basis functions, a recursive formulae is used; higher order basis functions are calculated from lower order basis functions. The B-spline basis function for the first order polynomial and for the higher order polynomials (p≥1) are given by (Boor 1972)

$$\phi_{i,p}(x) = \frac{(x - x_i)}{(x_{i+p} - x_i)} \phi_{i,p-1}(x) + \frac{(x_{i+p+1} - x)}{(x_{i+p+1} - x_{i+1})} \phi_{i+1,p-1}(x) \tag{29}$$

The basis functions for the linear polynomials (p=1) and for the quadratic polynomials (p=2) are given by

$$\phi_{i,1}(x) = \frac{(x - x_i)}{(x_{i+1} - x_i)} \phi_{i,0}(x) + \frac{(x_{i+2} - x)}{(x_{i+2} - x_{i+1})} \phi_{i+1,0}(x) \tag{30}$$

$$\phi_{i,2}(x) = \frac{(x - x_i)}{(x_{i+2} - x_i)} \phi_{i,1}(x) + \frac{(x_{i+3} - x)}{(x_{i+3} - x_{i+1})} \phi_{i+1,1}(x) \tag{31}$$

Figs. 2(a)-(b)-(c) show constant, linear, and quadratic B-spline curves, respectively (Hughes *et al.* 2005). Where the knot vector [x] is given by

$$[x] = [1 \quad 2 \quad 3 \quad 4 \quad 5]$$

We can clearly see from the Figs. 2(a)-(b)-(c) that the n^{th} order B-spline curve will contribute to n+1 sub-intervals.

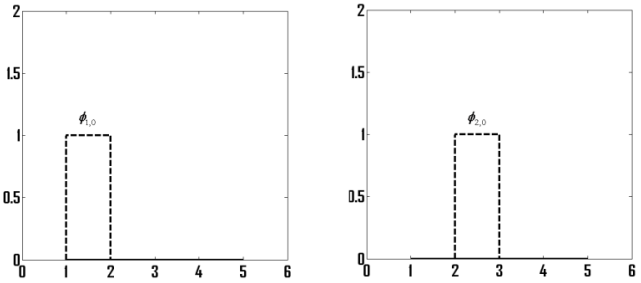

Fig. 2(a) Constant B-spline curves

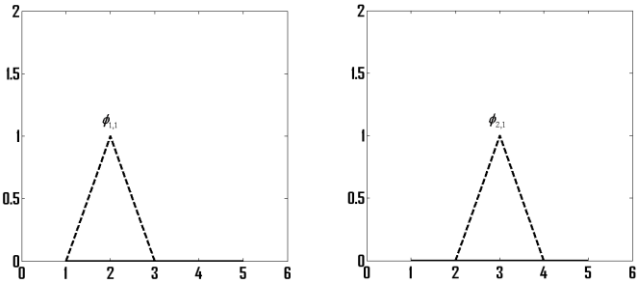

Fig. 2(b) Linear B-spline curves

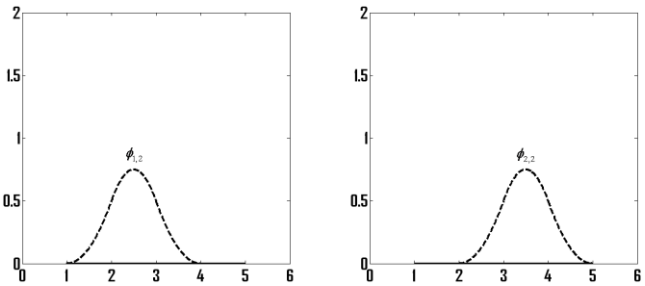

Fig. 2(c) Quadratic B-spline curves s

From Eqs. (28), (30), and (31), we write the quadratic B-spline equation, which includes three subintervals

$$[\phi_i] = \frac{1}{2h^2} \begin{cases} (x - x_i)^2 \\ (x - x_i)(x_{i+2} - x) + (x_{i+3} - x)(x - x_{i+1}) \\ (x_{i+3} - x)^2 \end{cases} \quad \begin{matrix} [x_i, x_{i+1}] \\ [x_{i+1}, x_{i+2}] \\ [x_{i+2}, x_{i+3}] \end{matrix} \tag{32}$$

The quadratic B-spline basis function is a lower order polynomial when compared to the Hermite cubic polynomials. In polynomial order, the cubic B-spline basis function is equivalent to the Hermite cubic polynomials, but for the later, the second derivative of the field variable is not continuous.

The components of the quadratic B-spline basis function for a subinterval [x_i–x_{i+1}] are given as

$$\begin{bmatrix} \phi_{i-2} \\ \phi_{i-1} \\ \phi_i \end{bmatrix} = \frac{1}{2h^2} \begin{bmatrix} (x_{i+1} - x)^2 \\ (x - x_{i-1})(x_{i+1} - x) + (x_{i+2} - x)(x - x_i) \\ (x - x_i)^2 \end{bmatrix} \tag{33}$$

It is clear from Eq. (33) that three B-spline curves will

contribute to one sub-interval. And one can approximate the transverse displacement (field variable) in this sub-interval using the basis function given by

$$\overline{w}_{(i,i+1)} = \phi_{i-2}\beta_{i-2} + \phi_{i-1}\beta_{i-1} + \phi_i\beta_i \tag{34}$$

$$\overline{w}_{(i,i+1)} = [\phi]_{(i,i+1)}[\beta]_{(i,i+1)} \tag{35}$$

where β_1, β_2, β_3,…, β_n are the unknown B-spline curve parameters.

The equivalent approximation in the conventional finite element is given by

$$\overline{w}_{(i,i+1)} = [N]_{(i,i+1)}[d]_{(i,i+1)} \tag{36}$$

where, vector [d] contains twice the number of unknowns than in vector [β] A total of n unknowns will appear with Eq. (35), but the conventional finite element method yields $2n$ unknowns after the application of the essential boundary conditions and hence the size of matrices will be double in the conventional finite element method.

Weak formulation can be obtained over a sub-interval. Using Galerkin's method, for interval [x_i–x_{i+1}] we get the stiffness matrix as

$$[K]_{(i,i+1)} = \int_{x_i}^{x_{i+1}} g(\zeta)\frac{d^2[\phi]^T_{(i,i+1)}}{d\zeta^2}\frac{d^2[\phi]_{(i,i+1)}}{d\zeta^2}d\zeta + \int_{x_i}^{x_{i+1}} s^2 h(\zeta)\frac{d[\phi]^T_{(i,i+1)}}{d\zeta}\frac{d[\phi]_{(i,i+1)}}{d\zeta}d\zeta - \int_{x_i}^{x_{i+1}} \frac{s^2}{r^2} g(\zeta)\frac{d[\phi]^T_{(i,i+1)}}{d\zeta}\frac{d[\phi]_{(i,i+1)}}{d\zeta}d\zeta \tag{37}$$

and the mass matrix as

$$[M]_{(i,i+1)} = \int_{x_i}^{x_{i+1}} f(\zeta)[\phi]^T_{(i,i+1)}[\phi]_{(i,i+1)}d\zeta + \int_{x_i}^{x_{i+1}} \frac{1}{r^2} g(\zeta)\frac{d[\phi]^T_{(i,i+1)}}{d\zeta}\frac{d[\phi]_{(i,i+1)}}{d\zeta}d\zeta \tag{38}$$

The B-spline approximation does not satisfy the Kronecker delta property and a transformation matrix is used to apply the essential boundary conditions. The transformation is given by

$$\begin{bmatrix} \overline{w}(0) \\ \overline{w}'(0) \\ \beta_0 \\ \beta_1 \\ . \\ . \\ \beta_n \end{bmatrix} = \begin{bmatrix} \phi_{-2} & \phi_{-1} & \phi_0 & 0 & 0 & 0 & 0 \\ \phi'_{-2} & \phi'_{-1} & \phi'_0 & 0 & 0 & 0 & 0 \\ 0 & 0 & 1 & 0 & 0 & 0 & 0 \\ 0 & 0 & 0 & 1 & 0 & 0 & 0 \\ 0 & 0 & 0 & 0 & . & 0 & 0 \\ 0 & 0 & 0 & 0 & 0 & . & 0 \\ 0 & 0 & 0 & 0 & 0 & 0 & 1 \end{bmatrix} \begin{bmatrix} \beta_{-2} \\ \beta_{-1} \\ \beta_0 \\ \beta_1 \\ . \\ . \\ \beta_n \end{bmatrix} \tag{39}$$

$$\Rightarrow [w] = [T][\beta]$$
$$\Rightarrow [\beta] = [T]^{-1}[w] \tag{0}$$

where, [T] is a transformation matrix. We can see that the essential boundary conditions can be easily applied as the first two elements of vector [w] represent displacement and slope at the fixed node (In case of the cantilever boundary conditions).

Table 1 Non-dimensional natural frequencies of a non-rotating Rayleigh beam with linear area and cubic inertia variation

	r=10, s=0, $\overline{n}$ =1, c=1/2			r=100, s=0, $\overline{n}$ =1, c=1/2			
	(Banerjee and Jackson 2013)	FEM n=40	B-spline FEM m=40	(Banerjee and Jackson 2013)	FEM n=40	B-spline FEM m=40	FEM (n=40) (Euler-Bernoulli)
λ_1	3.7727	3.7727	3.7728	3.8233	3.8233	3.8234	3.8238
λ_2	17.097	17.0975	17.1079	18.304	18.3038	18.3153	18.3173
λ_3	40.412	40.4126	40.4794	47.178	47.1781	47.2599	47.2649
λ_4	N/A	69.4402	69.6629	N/A	90.1371	90.4422	90.4509
λ_5	N/A	101.4261	101.9597	N/A	147.1728	147.9916	148.0035

Table 2 Non-dimensional natural frequencies of a rotating Rayleigh beam with linear area and cubic inertia variation

	r=10, s=5, $\overline{n}$ =1, c=1/2			r=100, s=5, $\overline{n}$ =1, c=1/2			
	(Banerjee and Jackson 2013)	FEM n=40	B-spline FEM m=40	(Banerjee and Jackson 2013)	FEM n=40	B-spline FEM m=40	FEM (n=40) (Euler-Bernoulli)
λ_1	6.6118	6.6118	6.6120	6.7421	6.7421	6.7423	6.7434
λ_2	20.356	20.3563	20.3655	21.888	21.8883	21.8985	21.9053
λ_3	43.444	43.4436	43.5061	50.839	50.8391	50.9161	50.9339
λ_4	N/A	72.2411	72.4555	N/A	93.8788	94.1374	94.2067
λ_5	N/A	103.9772	104.4983	N/A	150.9629	151.7639	151.8160

5. Results and discussion

Results are obtained for the cantilever boundary conditions given by

$$\overline{w}_{(x=0)} = 0,\ \frac{d\overline{w}}{dx}_{(x=0)} = 0,\ V_{(x=R)} = 0,\ \text{and}\ M_{(x=R)} = 0.$$

where V is the shear force, and M is the bending moment.

For results, we consider a total of 40 subintervals for the quadratic B-spline finite element method and 40 elements for the conventional finite element method. The size of mass and stiffness matrix for the quadratic B-spline finite element method is [40,40] and for the conventional finite element it is [80,80] Results are obtained for a non-rotating (s=0) and a rotating beam (s=50)

Tables 1 and 2 show the first five non-dimensional natural frequencies of a non-rotating Rayleigh beam and a rotating Rayleigh beam, respectively. In both the Tables, the factor $\overline{n}$ which is responsible for the non-uniform nature of the beam is considered equal to 1. This leads to a cubic variation in $I(x)$ and a linear variation in $A(x)$ (Eqs. (19), (20)). The taper ratio c is chosen as 0.5. Two values of the slenderness ratio (r=10, r=100) are considered in both the Tables. The last column in both the Tables shows the results for an Euler-Bernoulli beam, and results are independent of the slenderness ratio. We see that the B-spline finite element method results compare well with the published results.

Table 3 Non-dimensional natural frequencies of a non-rotating Rayleigh beam with quadratic area and quartic inertia variation

	r=10, s=0, $\bar{n}$ =2, c=1/2			r=100, s=0, $\bar{n}$ =2, c=1/2			
	(Banerjee and Jackson 2013)	FEM n=40	B-spline FEM m=40	(Banerjee and Jackson 2013)	FEM n=40	B-spline FEM m=40	FEM (n=40) (Euler-Bernoulli)
λ_1	4.5517	4.5517	4.5518	4.6244	4.6244	4.6245	4.6251
λ_2	18.211	18.2107	18.2215	19.533	19.5328	19.5447	19.5476
λ_3	41.457	41.4573	41.5253	48.489	48.4886	48.5717	48.5790
λ_4	N/A	70.3744	70.5995	N/A	91.4925	91.8002	91.8132
λ_5	N/A	102.2365	102.7736	N/A	148.5498	149.3729	149.3917

Table 4 Non-dimensional natural frequencies of a rotating Rayleigh beam with quadratic area and quadratic inertia variation

	r=10, s=5, $\bar{n}$ =2, c=1/2			r=100, s=5, $\bar{n}$ =2, c=1/2			
	(Banerjee and Jackson 2013)	FEM n=40	B-spline FEM m=40	(Banerjee and Jackson 2013)	FEM n=40	B-spline FEM m=40	FEM(n=40) (Euler-Bernoulli)
λ_1	7.1268	7.1268	7.1269	7.2885	7.2885	7.2886	7.2901
λ_2	21.003	21.0033	21.0129	22.618	22.6179	22.6286	22.6360
λ_3	44.014	44.0143	44.0786	51.595	51.5945	51.6735	51.6919
λ_4	N/A	72.7026	72.9205	N/A	94.6302	94.9289	94.9630
λ_5	N/A	104.3394	104.8659	N/A	151.7073	152.5153	152.5683

For the non-uniform parameter $\bar{n} = 2$, results are obtained in Tables 3 and 4, and every other parameter is kept same as shown in Tables 1 and 2. This case corresponds to a quartic variation in $I(x)$ and a quadratic variation in $A(x)$. Tables 3 and 4 show the first five non-dimensional natural frequencies of a non-rotating Rayleigh beam and a rotating Rayleigh beam, respectively. Again, we see that the B-spline finite element method compared well with the published results. The first five mode shapes are drawn in Figs. 3 and 4 for the values of $\bar{n}$ equal to 1 and 2, respectively.

In Fig. 5, the fifth natural frequency is plotted with the change in slenderness ratio for non-uniform parameter $(\bar{n})$ equal to 1. We can clearly see that for higher slenderness ratio, higher natural frequencies of Rayleigh beam and Euler-Bernoulli beam are almost equal. For lower modes, natural frequencies are almost equal in both the theories (negligible variation with the change in the slenderness ratio); from the analytical solutions of non-rotating beams, one can clearly see that the effect of the rotary inertia term is not prominent for lower modes.

The non-uniform parameter $(\bar{n})$ is varied to get change inthe first five natural frequencies. The results are shown in the Table 5, where all the five natural frequencies vary linearly with linear change in non-uniform parameter, which can be observed in the Fig. 6.

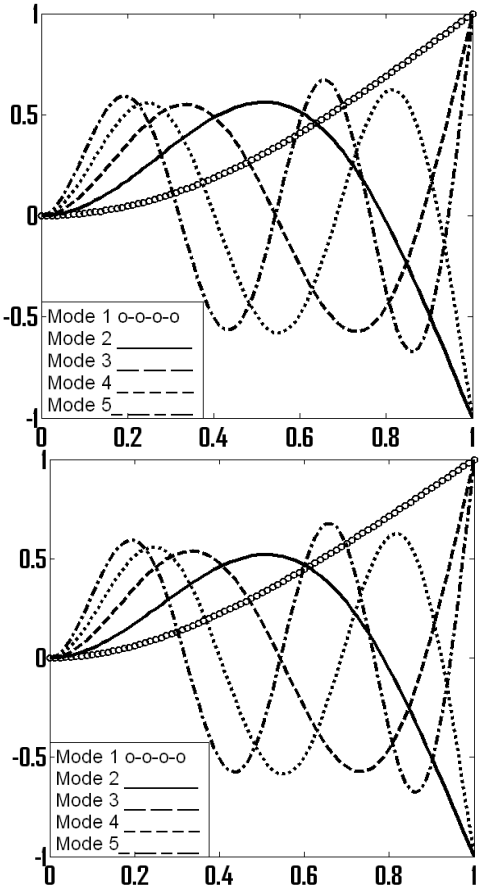

Figs. 3(a)-(b) Mode shapes of a non-rotating and a rotating beam for $\bar{n} = 1$, respectively (linear area and cubic inertia variation)

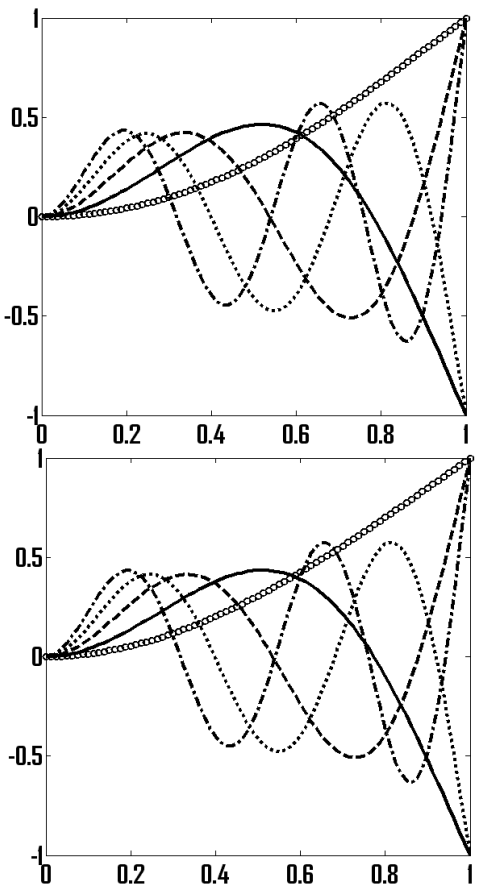

Figs. 4(a)-(b)Mode shapes of a non-rotating and a rotating beam for $\bar{n} = 2$, respectively (quadratic area and quartic inertia variation)

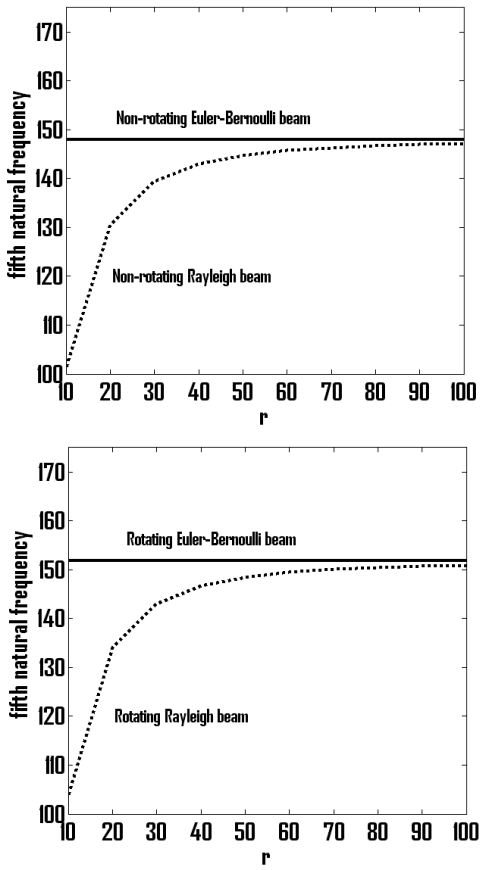

Figs. 5(a)-(b) Variation in the fifth natural frequency with change in the slenderness ratio for a non-rotating and a rotating beam, respectively

Table 5 Variations in the first five natural frequencies with change in non-uniform parameter

r=10, s=0, c=1/2	$\bar{n}=1$	$\bar{n}=2$	$\bar{n}=3$	$\bar{n}=4$	$\bar{n}=5$
λ_1	3.7728	4.5518	5.4416	6.4470	7.5712
λ_2	17.1079	18.2215	19.4045	20.6639	22.0059
λ_3	40.4794	41.5253	42.6525	43.8610	45.1511
λ_4	69.6629	70.5995	71.6133	72.7031	73.8680
λ_5	101.9597	102.7736	103.6581	104.6121	105.6344

6. Conclusions

Rayleigh beams include the effect of rotary inertia besides retaining the usual assumptions made for Euler-Bernoulli beams. Rayleigh rotating beam models are finding increasing use in engineering structures such as helicopter rotor blades, compressor and turbine blades. Calculating accurate frequencies and mode shapes of the rotating structure in a computationally efficient manner plays an important role in their design. The free vibration problem of a rotating Rayleigh beam is solved with the quadratic B-spline finite element method. The size of the matrices and lower polynomial order are of importance with this method as matrix inversion becomes easier and requires less computational effort. Results are also obtained with the conventional finite element method with an equivalent discretization; total 40 elements in comparison to 40 sub-intervals of the quadratic B-spline finite element method. Results show an accurate match with the results published in literature and with the conventional finite element results for different non-uniform cross sections. In particular, two cases on non-uniform parameter $\bar{n}=1$ and $\bar{n}=2$ are considered which correspond to linear area and cubic inertia variation, and quadratic area and quartic inertia variation, respectively. The non-uniform beam formulation developed in this paper is valid for a large classes of practical beams. Results are also obtained with the Euler-Bernoulli beam theory to see the effect of slenderness ratio $\left(\sqrt{A_0R^2/I_0}\right)$ on the Rayleigh beam results. It is evident that for higher modes at higher slenderness ratio, the results of both the theories are almost equal. Also, variations in first five natural frequencies are obtained with change in non-uniform parameter.

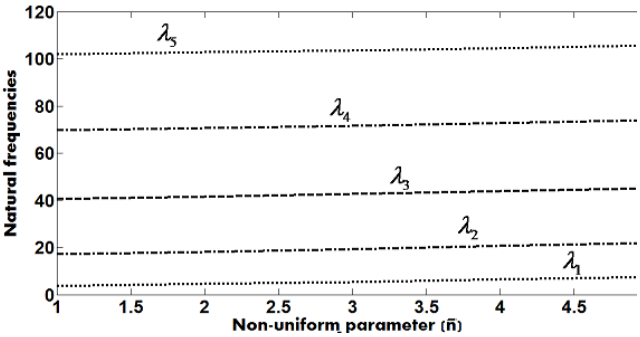

Fig. 6 Variations in the first five natural frequencies with change in non-uniform parameter

References

Auciello, N.M. (2013), "Dynamics analysis of rotating tapered beams using two general approaches", *Proceedings of the Electronic International Interdisciplinary Conference,* Zillina, September.

Avcar, M. (2015), "Effects of rotary inertia, shear deformation and non-homogeneity on frequencies of beam", *Struct. Eng. Mech.*, **55**, 871-884.

Banerjee, J.R. and Jackson, D.R. (2013), "Free vibration of a rotating tapered Rayleigh beam: A dynamic stiffness method of solution", *Comput. Struct.*, **124**, 11-20.

Bauchau, O.A. and Hong, C.H. (1987), "Finite element approach to rotor blade modeling", *J. Am. Helic. Soc.*, **32**, 60-67.

Bokaian, A. (1990), "Natural frequencies of beams under tensile axial loads", *J. Sound Vib.*, **142**, 481-498.

Boor, C.D. (1972), "On calculating with B-splines", *J. Approx. Theory*, **6**, 50-62.

Bornemann, P.B. and Cirak, F. (2013), "A subdivision-based implementation of the hierarchical B-spline finite element method", *Comput. Meth. Appl. Mech. Eng.*, **253**, 584-598.

Dag, I. and Ozer, M.N. (2001), "Approximation of the RLW equation by the least square cubic B-spline finite element method" *Appl. Math. Model.*, **25**, 221-231.

Gardner, L.R.T., Gardner, G.A. and Dag, I. (1995), "A B-spline finite element method for regularized long wave equation", *Commun. Numer. Meth. Eng.*, **11**, 59-68.

Giurgiutiu, V. and Stafford, R.O. (1977), "Semi-analytical methods for frequencies and mode shapes of rotor blades", *Vertica*, **1**, 291-306.

Gupta, A., Kiusalaas, J. and Saraph, M. (1991), "Cubic B-spline for finite element analysis of axisymmetric shells", *Comput. Struct.*, **38**, 463-468.

Hoa, S.V. (1979), "Vibration of a rotating beam with tip mass", *J. Sound Vib.*, **167**, 369-381.

Hodges, H.D. and Rutkowski, M.J. (1981), "Free-vibration analysis of rotating beams by a variable-order finite element method", *AIAA J.*, **19**, 1459-1466.

Hughes, T.J.R., Cottrell, J.A. and Bazilevs, Y. (2005), "Isogeometric analysis: CAD, finite elements, NURBS, exact geometry and mesh refinement", *Comput. Meth. Appl. Mech. Eng.*, **194**, 4135-4195.

Kagan, P., Fischer, A. and Bar-Yoseph, P.Z. (1998), "New B-spline finite element approach for geometric design and mechanical analysis", *Int. J. Numer. Meth. Eng.*, **41**, 435-458.

Mao, Q. (2015), "AMDM for free vibration analysis of rotating tapered beams", *Struct. Eng. Mech.*, **54**, 419-432.

Mohammadi, R. (2014), "Sextic B-spline collocation method for solving Euler-Bernoulli beam models", *Appl. Math. Comput.*, **241**, 151-166.

Mohammadnejad, M. (2015), "A new analytical approach for determination of flexural, axial and torsional natural frequencies of beams", *Struct. Eng. Mech.*, **55**, 655-674.

Nagaraj, V. T. and Shanthakumar, P. (1975), "Rotor blade vibration by the Galerkin finite element method", *J. Sound Vib.*, **43**, 575-577.

Reddy, J.N. (2005), *An Introduction to the Finite Element Method*, Tata McGraw-Hill, New York, USA.

Rostami, S., Shojaee, S. and Saffari, H. (2013), "An explicit time integration method for structural dynamics using cubic B-spline polynomial functions", *Scientia Iranica*, **20**, 23-33.

Sarkar, K., Ganguli, R. and Elishakoff, I. (2016), "Closed-form solutions for non-uniform axially loaded Rayleigh cantilever beams", *Struct. Eng. Mech.*, **60**, 455-470.

Shen, L., Liu, Z. and Wu, J.H. (2014), "B-spline finite element method based on node moving adaptive refinement strategy", *Finite Elem. Anal. Des.*, **91**, 84-94.

Shen, P.C. and Wang, J.G (1987), "Static analysis of cylindrical shells by using B-spline functions", *Comput. Struct.*, **25**, 809-816.

Tang, A.Y., Li, X.F., Wu, J.X. and Lee, K.Y. (2015), "Flapwise bending vibration of rotating tapered Rayleigh cantilever beams", *J. Constr. Steel Res.*, **112**, 1-9.

Wang, G. and Wereley, N.M. (2004), "Free vibration analysis of rotating blades with uniform tapers", *AIAA J.*, **42**, 2429-2437.

Zeid, I. (2007), *Mastering CAD/CAM*, Tata McGraw-Hill, New York, USA.

CC